Available online at www.sciencedirect.com

ScienceDirect

Procedia Structural Integrity 68 (2025) 1074–1080

Structural Integrity Procedia

www.elsevier.com/locate/procedia

European Conference on Fracture 2024

Hydrogen interaction with post-processed L-PBF 316L stainless steel

Liesbet Deconinck[a]*, Pedro A. Ferreirós[b], Zaiqing Que[b]*, Roy Johnsen[a], Xu Lu[a]*

[a] *Norwegian University of Science and Technology (NTNU), Department of Mechanical and Industrial Engineering, Richard Birkelands vei 2B, N-7034 Trondheim, Norway*

[b] *VTT Technical Research Centre of Finland, Kivimiehentie 3, 02150 Espoo, Finland*

Abstract

Additive manufacturing (AM) offers multiple economic and ecologic advantages with respect to the conventional manufacturing techniques. Post-processing treatments are typically applied to further improve the AM material's performance for industrial applications. However, knowledge is still lacking about the hydrogen interaction with these specific post-processed AM microstructures. Therefore, this research focuses on the hydrogen embrittlement of stress relieved (SR) and hot isostatic pressed (HIP) laser powder bed fused (L-PBF) 316L austenitic stainless steel. An in-depth characterization is performed to examine the degradation of L-PBF 316L upon galvanostatic hydrogen charging, using complementary identification techniques. The results show that the microstructure determines the interaction with hydrogen, which regulates the hydrogen uptake capacity. The SR L-PBF 316L has an underlying substructure consisting of dislocation cells, whereas HIP L-PBF 316L largely resembles conventionally processed 316L stainless steel. Furthermore, it is observed that hydrogen charging introduces slip bands and lattice strains in both microstructures. As a result, the L-PBF 316L microstructure can be tuned by a specific post-processing treatment for an optimal resistance against hydrogen assisted degradation.

Keywords: 316L; Laser powder bed fusion; Stress relieve; Hot isostatic pressing; Hydrogen embrittlement

* Corresponding authors.
E-mail addresses: liesbet.deconinck@ntnu.no, zaiqing.que@vtt.fi, xu.lu@ntnu.no.

10.1016/j.prostr.2025.06.172

1. Introduction

As known since a long time, hydrogen embrittlement (HE) poses a significant challenge for metallic materials exposed to hydrogen environments (Johnson, 1875). It can lead to a premature degradation in ductility and reduction in fracture toughness for diverse applications. As a mitigation for this widespread problem, the material choice is important. Austenitic stainless steels (ASS) are reported to show a relatively lower susceptibility to hydrogen embrittlement than other types of steel (San Marchi & Somerday, 2014). ASS are of interest due to their decent mechanical properties and high corrosion resistance, even at elevated temperatures (Parr & Hanson, 1965). Furthermore, the 316L ASS shows a low hydrogen diffusivity and a high hydrogen solubility in hydrogen environments, qualifying for the use in hydrogen infrastructure. The interaction between hydrogen and conventionally manufactured 316L stainless steel is widely explored (Eliezer, 1984). It has been demonstrated that hydrogen reduces the stacking fault energy. Besides, hydrogen facilitates the formation of martensite, embrittling the structure (Narita et al., 1982).

Meanwhile, additive manufacturing (AM) is gaining attention compared to the conventional manufacturing techniques. This fabrication technique can produce high strength properties, while enabling complex geometries with a lower energy consumption and material waste than conventional manufacturing (Abd-Elaziem et al., 2022). A common AM production process is laser powder bed fusion (L-PBF), where a laser repeatedly and selectively melts a layer of powder. This AM fabrication process introduces particular microstructural features, related to the high cooling rate and restricted solidification direction. Examples include residual stresses, cellular dislocation cells, melt pool boundaries, and anisotropic material properties (Li et al., 2024). As a result, the mechanical strength of as-built L-PBF structures is higher than that of conventionally manufactured steels (Bartolomeu et al., 2017).

It is widely reported that the microstructure of a material determines its interaction with hydrogen. Therefore, the processing method contributes to the susceptibility to hydrogen embrittlement. As an example, recent literature reported that as-built L-PBF 316L ASS shows an equal or better resistance to hydrogen embrittlement than conventionally manufactured 316L (Álvarez et al., 2023; Baek et al., 2017; Claeys et al., 2023). Multiple explanations are attributed to this observation. Bertsch et al. highlighted that the morphology and spacing of the dislocation structures are responsible for the resistance to hydrogen embrittlement in L-PBF 316L (Bertsch et al., 2021). Álvarez et al. showed that the hydrogen resistance in L-PBF 316L is improved by a reduced propensity to form strain induced martensite because the austenite phase is stabilized (Álvarez et al., 2023). Additionally, Claeys et al. reported that the corresponding hydrogen diffusivity and hydrogen solubility strongly differs, depending on the microstructure (Claeys et al., 2023).

However, the microstructure changes again after applying a post-processing treatment on the L-PBF 316L. Post-processing treatments are typically applied to further improve the AM material's performance for industrial applications. Nevertheless, profound knowledge is still lacking about the hydrogen interaction with specific post-processed AM microstructures. Therefore, this research focuses on the hydrogen interaction with stress relieved (SR) and hot isostatic pressed (HIP) L-PBF fused grade 316L ASS.

2. Materials and methods

The samples were manufactured by L-PBF with an EOS M290. The chemical composition of the 316L stainless steel powder is given in Table 1. The printing parameters were optimized to minimize the degree of porosity. The specimens were printed in a vertical direction. The detailed printing and laser parameters are described by Que et al. (Que et al., 2022).

Two post-processing conditions were investigated. The first one was SR of the as-built L-PBF 316L specimens, obtained by holding the samples for 2 hours at 650 °C in argon atmosphere, followed by air cooling. The second condition included HIP of specimens following the stress relieving treatment. The HIP parameters consisted of keeping the material for 4 hours at 1150 °C in 100 MPa argon atmosphere, followed by furnace cooling.

Table 1: Chemical composition of the 316L austenitic stainless steel powder.

Element	[wt%]
Chromium	17.7
Nickel	12.6
Molybdenum	2.3
Manganese	0.5
Silicon	0.67
Nitrogen	0.09
Copper	<0.01
Sulphur	0.005
Phosphor	0.008
Iron	Balance

Hydrogen charging was performed galvanostatically in a three-electrode set-up for 24 hours at 60 °C. The current density was kept constant at -10 $mA \cdot cm^{-2}$ in 1:2 vol% phosphoric acid with glycerol, using a Ag/AgCl reference electrode and a platinum counter electrode.

The total hydrogen content was determined by hot extraction with a Bruker Phoenix G4. The sample was quickly heated up to 800 °C and kept at this temperature for 10 minutes before applying furnace cooling. The thermal conductivity detector measured the difference in thermal conductivity between the liberated hydrogen and the nitrogen carrier gas.

The microstructural investigation was performed with a FEI Quanta 650 secondary electron microscope (SEM) at an acceleration voltage of 20 kV. The Everhart-Thornley detector with secondary electron detection was used, complementary to the backscattered electron detector. Besides, this device was used for electron backscattered diffraction (EBSD) for complementary microstructural identification. The specimen was tilted 70°.

The present crystallographic phases and introduced stresses were identified by X-ray diffraction (XRD). A Bruker D8 A25 DaVinci with Cu-Kα source was operated at an accelerating current of 40 mA and an acceleration voltage of 40 kV. The scanning angle 2θ ranged from 40 to 95°.

Tensile tests were conducted in a Kammrath &Weiss tensile-compression module at a strain rate of 10^{-4} s^{-1}. The tensile specimens had a gage length of 10 mm, and the building direction was parallel to the loading direction. The samples were precharged with the abovementioned parameters.

3. Results & discussion

The significantly different microstructures of the SR and the HIP L-PBF 316L are shown in Figure 1 and Figure 2. The goal of the SR procedure is to reduce the residual stresses introduced by the L-PBF fabrication process. The SR microstructure did not significantly rearrange compared to the as-built condition. The directional grains are clearly visible. This microstructure has a cellular substructure, intrinsic to the fast cooling rates in the fabrication process (Lin et al., 2020). On the other hand, the HIP L-PBF 316L microstructure demonstrates rather equiaxed grains, with annealing twins present. The high temperature and pressure rearranged the grain structure to a similar appearance as known from conventionally manufactured 316L despite a smaller grain size and a higher fraction of low-angle grain boundaries (Que et al., 2022). Meanwhile, the underlying cellular dislocation structure was largely resolved by the HIP treatment. No lack-of-fusion pores were observed in any of the cases.

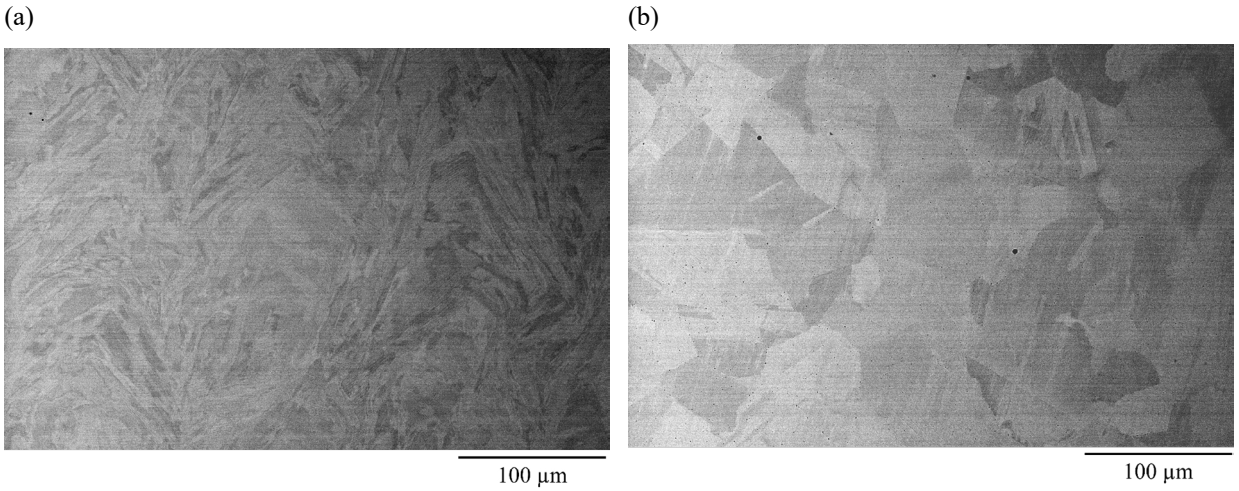

Figure 1: SEM micrograph from (a) SR and (b) HIP L-PBF 316L. The building direction is oriented horizontally in both cases.

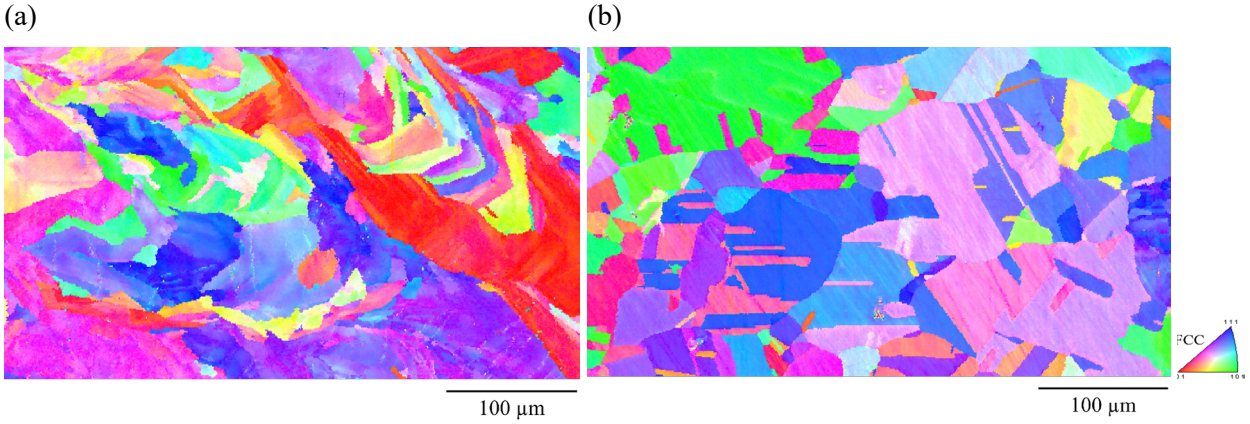

Figure 2: EBSD figures of (a) SR and (b) HIP L-PBF 316L. The building direction is oriented horizontally in both cases.

The effect of hydrogen charging on the different microstructures was first evaluated with XRD. The XRD patterns of both post-processing conditions are given in Figure 3, before and after electrochemical hydrogen charging. The face centered cubic austenite phase was present in all conditions.

Comparing the uncharged materials reveals that the peaks of uncharged HIP L-PBF 316L are narrower than for uncharged SR L-PBF 316L. This observation confirms that the HIP treatment reduces the quantity of residual stresses compared to the SR treatment, due to the additional cycle at high temperature and high pressure.

Upon hydrogen charging, the characteristic peaks broaden with respect to the uncharged condition, and slightly shift to lower 2θ angles. The observed peak broadening indicates that hydrogen introduces non-uniform stresses in the microstructure. Considering the charged microstructure micrographs in Figure 4 with slip bands, the broader peak appearance upon hydrogen charging can also be related to the scattering of the coherently diffracting slip bands, in combination with dislocation scattering. Besides, the slight peak shift to the left upon hydrogen charging indicates an expansion of the lattice constant due to the introduction of interstitial hydrogen atoms. No additional phases were observed with XRD after hydrogen charging. In contrast, conventionally manufactured 316L steel typically undergoes a partial phase transformation into martensite upon hydrogen charging (Metalnikov et al., 2022).

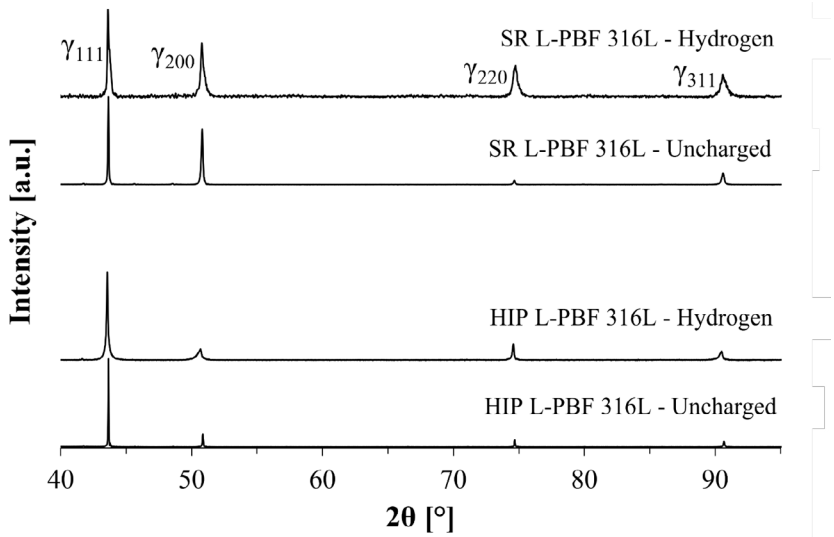

Figure 3: X-ray diffraction spectrum of L-PBF 316L ASS. SR and HIP L-PBF 316L are compared, both without and with hydrogen charging. Hydrogen introduces peak broadening in both post-processing conditions.

After hydrogen charging, the surface integrity was clearly affected. As shown in Figure 4, hydrogen introduces parallel slip lines in both post-processing conditions. The direction of the slip bands depended on the grain orientation. Some orientations demonstrated two orientations of slip lines. Besides, minor crack formation was observed, aligned with the slip bands (but not shown in the figure). On the other hand, the small number of pre-existing porosities did not show interaction with hydrogen.

The hydrogen induced slip band formation has been observed before in other microstructures, e.g. in nickel and high entropy alloys (Lu et al., 2019; Wang et al., 2019). Ménard et al. investigated the morphology of hydrogen induced slip bands in conventionally manufactured 316L (Ménard et al., 2008). These authors observed hydrogen induced slip localization. They reported that the grain size determines the slip morphology, correlated to the internal stresses. In the current results, the grain size was lower than reported by these authors, resulting in a lower average slip band spacing. However, the actual slip band spacing was observed to be related to the grain orientation. The minimal observed slip band spacing was 0.5 µm for HIP L-PBF 316L and 0.3 µm for SR L-PBF 316L from the SEM micrographs. This is slightly larger than the minimal slip band spacing of 0.53 µm that Li et al. reported in hydrogenated as-built L-PBF 316L (Li et al., 2024). This slip band formation can help identifying the active mechanism for hydrogen assisted degradation in L-PBF 316L. Besides, Moody and Greulich reported in an Fe-Ni-Co superalloy that these slip bands form locations for crack initiation upon mechanical loading (Moody & Greulich, 1985).

The hot extraction results showed that the SR condition has a higher hydrogen uptake capacity than the HIP condition, 67.4 ± 11.6 wppm versus 37.2 ± 1.9 wppm hydrogen respectively. The difference in hydrogen interaction is related to the corresponding microstructure. The cellular subgrains are absent in HIP L-PBF 316L, while they support hydrogen uptake and transport in SR L-PBF 316L. Accordingly, Lin et al. reported that hydrogen preferentially moves along the cellular boundaries in as-built L-PBF 316L (Lin et al., 2020). Furthermore, Metalnikov et al. identified two hydrogen trapping sites in as-built L-PBF 316L, related on the one hand to the elastic stress field of a dislocation core, and on the other hand to the subgrain dislocation cell walls (Metalnikov et al., 2022). The current SR L-PBF 316L microstructure also has a similar cellular substructure that acts as hydrogen trapping site, explaining the higher hydrogen uptake capacity in SR L-PBF 316L compared to HIP L-PBF 316L (Que et al., 2022). However, the reported associated trapping energy is close to the irreversible trapping energy threshold, so it cannot be concluded that SR L-PBF 316L is more prone to hydrogen embrittlement than HIP L-PBF 316L. Further mechanical testing provides complementary information about the mechanism of hydrogen embrittlement in SR and HIP L-PBF 316L.

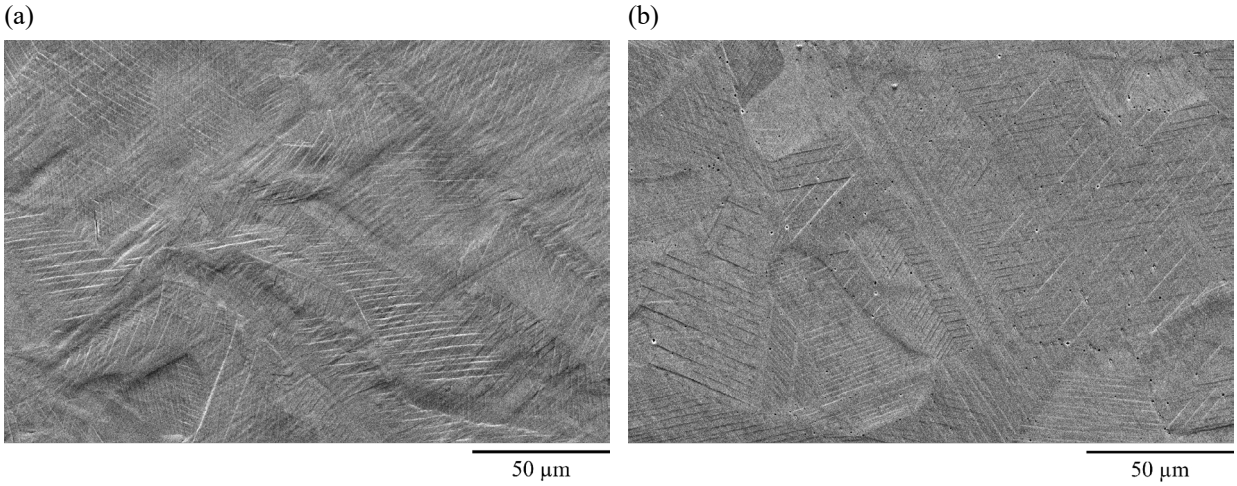

Figure 4: SEM micrograph after hydrogen charging. L-PBF 316L stainless steel with subsequent (a) SR and (b) HIP post-processing treatment. The building direction is oriented horizontally in both cases.

The hydrogen charged microstructures were subjected to tensile testing. The normal plane of the fractured hydrogenated SR and HIP L-PBF 316L is shown in Figure 5. Upon deformation, more slip lines are created, and additional secondary cracks appear. The crack pathway of the HIP L-PBF 316L is straight, whereas a serrated crack is observed in the SR condition. It is clearly visible that the cracks follow the slip lines, and mostly stop at the grain boundary for both conditions. The loading direction defined which grain orientations were more prone to cracking.

Similar as in conventionally manufactured 316L, hydrogen is assumed to reduce the stacking fault energy (Narita et al., 1982). The plastic deformation accumulates in the slip bands and forms a preferential crack initiation site. Furthermore, Li et al. discussed the role of slip bands in hydrogenated as-built L-PBF 316L (Li et al., 2024). They reported an enhanced dislocation motion upon hydrogen charging. The dislocations accumulate at the slip bands together with hydrogen atoms, which facilitates an embrittled cracking behavior. Similarly, Hong et al. demonstrated that hydrogen enhances the dislocation mobility and slip planarity in as-built L-PBF 316L ASS (Hong et al., 2022). The current observations tend towards indications that the HELP and HEDE mechanism are active in the hydrogen embrittlement of these SR and HIP L-PBF 316L microstructures.

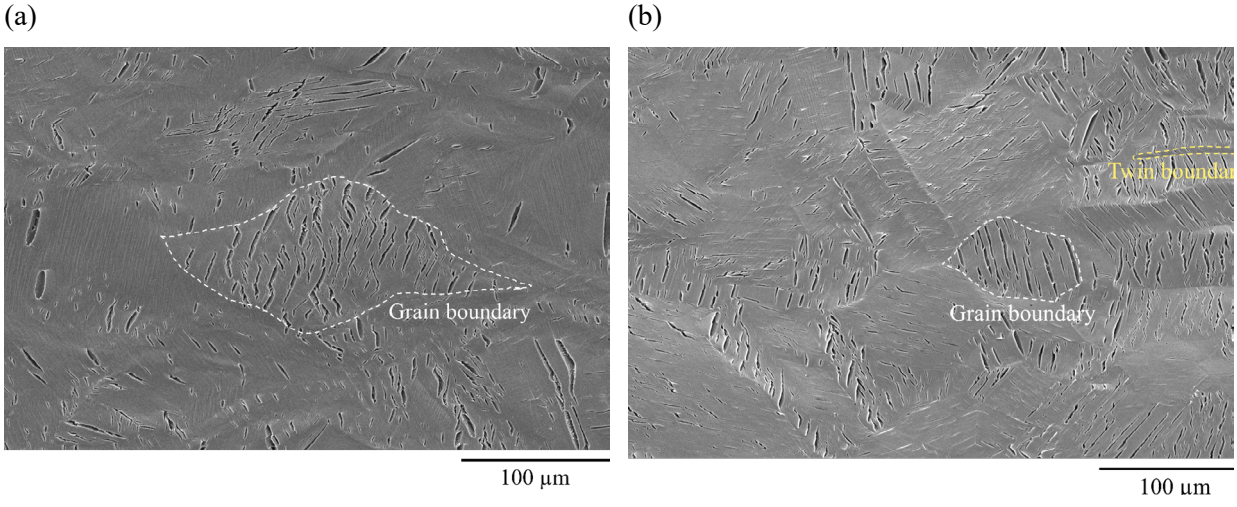

Figure 5: SEM micrograph of fractured (a) SR and (b) HIP L-PBF 316L ASS after hydrogen charging. The building direction and loading direction are oriented horizontally. The cracks align with the preformed slip lines. An example of a grain boundary and twin boundary are indicated, where the cracks are typically halted

4. Conclusions

AM introduces a completely different microstructure than the known conventional microstructures. By applying a particular post-processing treatment, a full spectrum of microstructures can be obtained. The resistance to hydrogen embrittlement can be largely tuned by adjusting the microstructure. Depending on the application, a specific post-processing treatment can be applied to obtain an optimal balance between mechanical properties and resistance to hydrogen assisted degradation. Nevertheless, hydrogen introduces slip localization in both SR and HIP L-PBF 316L. This affects subsequent crack initiation and propagation pathways. Therefore, understanding the dynamics between hydrogen and post-processed 316L enhances the reliability of these components in hydrogen-containing environments.

Acknowledgements

The authors would like to acknowledge the EU OFFERR HyAMsteel project. Besides, the authors are also grateful for the experimental work performed by Dr. Chandrahaasan Soundararajan in the project.

References

Abd-Elaziem, W., Elkatatny, S., Abd-Elaziem, A.-E., Khedr, M., El-baky, M. A. A., Hassan, M. A., Abu-Okail, M., Mohammed, M., Järvenpää, A., Allam, T., & Hamada, A. (2022). On the current research progress of metallic materials fabricated by laser powder bed fusion process: a review. *Journal of Materials Research and Technology*, *20*. https://doi.org/10.1016/j.jmrt.2022.07.085

Álvarez, G., Harris, Z., Wada, K., Rodríguez, C., & Martínez-Pañeda, E. (2023). Hydrogen embrittlement susceptibility of additively manufactured 316L stainless steel: Influence of post-processing, printing direction, temperature and pre-straining. *Additive Manufacturing*, *78*. https://doi.org/10.1016/j.addma.2023.103834

Baek, S.-W., Song, E. J., Kim, J. H., Jung, M., Baek, U. B., & Nahm, S. H. (2017). Hydrogen embrittlement of 3-D printing manufactured austenitic stainless steel part for hydrogen service. *Scripta Materialia*, *130*. https://doi.org/10.1016/j.scriptamat.2016.11.020

Bartolomeu, F., Buciumeanu, M., Pinto, E., Alves, N., Carvalho, O., Silva, F. S., & Miranda, G. (2017). 316L stainless steel mechanical and tribological behavior—A comparison between selective laser melting, hot pressing and conventional casting. *Additive Manufacturing*, *16*. https://doi.org/10.1016/j.addma.2017.05.007

Bertsch, K. M., Nagao, A., Rankouhi, B., Kuehl, B., & Thoma, D. J. (2021). Hydrogen embrittlement of additively manufactured austenitic stainless steel 316 L. *Corrosion Science*, *192*. https://doi.org/10.1016/j.corsci.2021.109790

Claeys, L., Deconinck, L., Verbeken, K., & Depover, T. (2023). Effect of additive manufacturing and subsequent heat and/or surface treatment on the hydrogen embrittlement sensitivity of 316L austenitic stainless steel. *International Journal of Hydrogen Energy*, *48*(92). https://doi.org/10.1016/j.ijhydene.2023.05.215

Eliezer, D. (1984). The behaviour of 316L stainless steel in hydrogen. *Journal of Materials Science*, *19*(5). https://doi.org/10.1007/BF00563051

Hong, Y., Zhou, C., Wagner, S., Schlabach, S., Pundt, A., Zhang, L., & Zheng, J. (2022). Strain-induced twins and martensite: Effects on hydrogen embrittlement of selective laser melted (SLM) 316 L stainless steel. *Corrosion Science*, *208*. https://doi.org/10.1016/j.corsci.2022.110669

Johnson, W. H. (1875). On Some Remarkable Changes Produced in Iron and Steel by the Action of Hydrogen and Acids. *Nature*, *11*(281). https://doi.org/10.1038/011393a0

Li, S.-H., Lee, D.-H., Zhao, Y., & Ramamurty, U. (2024). Hydrogen-induced softening and embrittlement in 316L stainless steel fabricated using laser-powder bed fusion. *Acta Materialia*, *274*. https://doi.org/10.1016/j.actamat.2024.119959

Lin, J., Chen, F., Liu, F., Xu, D., Gao, J., & Tang, X. (2020). Hydrogen permeation behavior and hydrogen-induced defects in 316L stainless steels manufactured by additive manufacturing. *Materials Chemistry and Physics*, *250*. https://doi.org/10.1016/j.matchemphys.2020.123038

Lu, X., Wang, D., Wan, D., Zhang, Z. B., Kheradmand, N., & Barnoush, A. (2019). Effect of electrochemical charging on the hydrogen embrittlement susceptibility of alloy 718. *Acta Materialia*, *179*. https://doi.org/10.1016/j.actamat.2019.08.020

Ménard, M., Olive, J. M., Brass, A.-M., & Aubert, I. (2008). Effects of hydrogen charging on surface slip band morphology of a type 316L stainless steel. In *Environment-Induced Cracking of Materials* (Vol. 1, pp. 179-188). https://doi.org/10.1016/B978-008044635-6.50017-0

Metalnikov, P., Ben-Hamu, G., Eliezer, D., Metalnikov, P., Ben-Hamu, G., & Eliezer, D. (2022). Hydrogen Trapping in Laser Powder Bed Fusion 316L Stainless Steel. *Metals 2022, Vol. 12, Page 1748*, *12*(10). https://doi.org/10.3390/met12101748

Moody, N. R., & Greulich, F. A. (1985). Hydrogen-induced slip band fracture in an Fe Ni Co superalloy. *Scripta Metallurgica*, *19*(9). https://doi.org/10.1016/0036-9748(85)90018-3

Narita, N., Altstetter, C. J., & Birnbaum, H. K. (1982). Hydrogen-related phase transformations in austenitic stainless steels. *Metallurgical Transactions A*, *13*(8). https://doi.org/10.1007/BF02642872

Parr, J. G., & Hanson, A. (1965). *An Introduction to Stainless Steel*. American Society for Metals.

Que, Z., Chang, L., Saario, T., & Bojinov, M. (2022). Localised electrochemical processes on laser powder bed fused 316 stainless steel with various heat treatments in high-temperature water. *Additive Manufacturing*, *60*. https://doi.org/10.1016/j.addma.2022.103205

San Marchi, C., & Somerday, B. P. (2014). Comparison of Stainless Steels for High-Pressure Hydrogen Service. ASME 2014 Pressure Vessels and Piping Conference, California, USA.

Wang, D., Lu, X., Deng, Y., Wan, D., Li, Z., & Barnoush, A. (2019). Effect of hydrogen-induced surface steps on the nanomechanical behavior of a CoCrFeMnNi high-entropy alloy revealed by in-situ electrochemical nanoindentation. *Intermetallics*, *114*. https://doi.org/10.1016/j.intermet.2019.106605